

Linear One-Dimensional Assembly of Metal Nanostructures onto an Asymmetric Peptide Nanofiber with High Persistence Length

Sudipta Mondal,* Pavel Rehak, Nandita Ghosh, Petr Král, and Ehud Gazit*



Cite This: *ACS Nano* 2022, 16, 18307–18314



Read Online

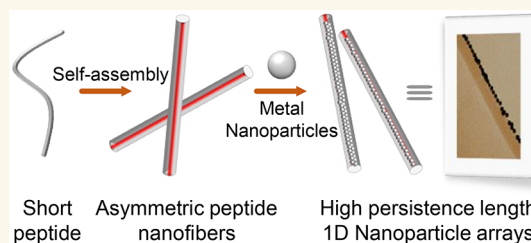
ACCESS |

Metrics & More

Article Recommendations

Supporting Information

ABSTRACT: Self-assembled peptide fibrils have been used extensively to template the organization of metal nanoparticles in a one-dimensional (1D) array. It has been observed that the formation of the 1D arrays with a width of a single or few nanoparticles (viz. 20 nm diameter) is only possible if the templating fibers have comparable diameters (viz. ≤ 20 nm). Accordingly, until today, all the peptide-based templates enabling such 1D arrays have very low persistence lengths, a property that depends strongly on the diameter of the template, owing to the inherent flexibility of only a few nanometer-wide fibers. Here, we demonstrate the formation of high persistence length 1D arrays templated by a short self-assembling peptide fibril with an asymmetrically distributed charged surface. The asymmetric nature of the peptide fibril allows charge-dependent deposition of the nanoparticles only to the part of the fiber with complementary charges, and the rest of the fibril surface remains free of nanoparticles. Consequently, fibers with a much higher diameter, which will have a higher persistence length, are able to template single or few nanoparticle-wide 1D arrays. Detailed microscopy, molecular dynamics simulations, and crystal structure analysis provide molecular-level insights into fiber asymmetry and its interactions with diverse nanostructures such as gold and magnetic nanoparticles. This study will afford an alternative paradigm for high persistence length 1D array fabrication comparable to DNA nanotechnology and lithography but with tremendous cost-effectiveness.



KEYWORDS: peptide self-assembly, one-dimensional nanoparticle arrays, asymmetric fibers, gold nanoparticles, magnetic nanoparticles

The assembly of metal nanoparticles in one- or quasi-one-dimensional (1D) architecture is one of the most extensively studied aspects of nanotechnology owing to their advantageous collective properties.^{1–3} 1D organization forms the basis of many advanced applications ranging from the plasmonic waveguides to surface enhanced Raman spectroscopy to optical metamaterials to enhanced magnetic effects.^{4–7} In a pioneering study, Maier and co-workers demonstrated plasmonic waveguides below the diffraction limit along the linear chain of nanoscale silver rods.⁸ These emerging applications inspire the development of diverse fabrication strategies. The top-down lithography represents a primary technique to produce nanoparticle arrays in which the length of the nanoparticle chain can be easily extended up to μm to mm scale.^{9–13} However, the fabrication of 1D chains with a width equal to the diameter of single or few nanoparticles with sizes well below 100 nm still possesses significant challenges.^{10–13} Templated assembly of nanoparticles is emerging as an advanced technique to afford coupled plasmonic nanoparticles at very high yields. The most advanced method employs bottom-up assembly of DNA to generate linear chain-like nanoparticle arrays with unparalleled

nanoscale precision.^{14–18} However, organization of DNA into high persistence length architecture is still challenging, and the recent advances in DNA origami allow formation of DNA nanostructures mostly around 1 μm long persistence length.¹⁷ Furthermore, DNA templated assembly requires extensive postsynthesis functionalization of metal nanoparticles, making the process cost-intensive.¹⁸

Self-assembling peptides represent another widely investigated bottom-up technology^{19–23} and have the potential to produce high aspect ratio 1D assembly in a cost-effective manner.^{24–26} Peptide nanofibers with diverse sequences and lengths have been explored to template metal nanoparticles in 1D architecture. In a recent study, it has been demonstrated that the co-incubation of gold salt with fibrils prepared from

Received: June 20, 2022

Accepted: November 3, 2022

Published: November 8, 2022



bacterial derived peptide leads to the dense coverage of the fibers with gold nanoparticles (AuNPs).²⁷ In another study, homogeneous coverage of AuNPs templated by cysteine modified coil-coiled peptide fibrils was achieved.²⁸ Very few reports have also described the formation of single nanoparticle-wide 1D arrays templated by peptide nanofibers.^{29–32} However, in later fabrication methods, the diameters of nanofiber and nanoparticle need to have comparable sizes, for example, to template 1D chains with 20 nm particles, one will need nanofibers with diameters of 20 nm or less. Thus, the templating of 1D arrays by peptide fibrils either lead to the complete coverage of the nanofibers and the number of nanoparticles wrapping the fibers increases with fibers diameters^{27,28,33–36} or to the formation of a 1D chain with one or few nanoparticles wide only when the nanofiber diameter is equal to or less than the nanoparticle sizes.^{24,29–32,37} Consequently, in the latter fabrication strategy, the peptide-based templates have a very low persistence length, a property that strongly depends on fiber diameter.³⁸ Here, we demonstrated the fabrication of single or few nanoparticle-wide 1D chains with several micrometers of persistence length templated by a short self-assembling peptide. The detail analysis also revealed that only a small fraction of the nanofiber surface is available toward nanoparticle attachment. Thus, fibers with a much larger diameter, which are expected to have higher persistence length, were able to template single or few nanoparticle-wide 1D chains. We performed an extensive analysis of the crystal structure of peptide nanofiber and implemented detailed all-atom molecular dynamics simulations to provide a molecular-level understanding of the assembly mechanism and established the electrostatic nature of the interactions between the nanoparticles and nanofibers. The nonspecific interactions allow us to align nanoparticles with diverse capping agents without any postsynthetic functionalization and to incorporate different types of nanoparticles such as gold and magnetic.

RESULTS AND DISCUSSION

Self-Assembly of Asymmetric Peptide Nanofibers.

Recently, we demonstrated the self-assembly of a short seven-residue sequence, termed as SHR-FF to nanofibers.^{39,40} Microcrystal X-ray diffraction of SHR-FF revealed the cross- β arrangement of the peptide in the nanofiber, confirming its amyloid-like characteristics.³⁹ As reported before, contrary to the extended conformation of the peptides in amyloid fibers composed of coded amino acids, SHR-FF adopted a looplike structure in which the C-terminal carboxyl group and N-terminal amine formed intramolecular H-bonding (Figure 1a). This pseudocyclic conformation of SHR-FF can be attributed to the presence of the 2-aminoisobutyric acid (Aib), a natural noncoded amino acid, that prefers non- β -sheet dihedral angles. An interesting feature of SHR-FF conformation, as observed in the crystal structure, is that although the peptide contains two polar serine residues, only the side chain of the residue located at the N-terminus (Ser1) was protruding outward of the cyclic-like conformation (Figure 1a). This phenomenon along with the outward exposure of only hydrophobic phenylalanine (Phe) and Aib side chains along the periphery resulted in the asymmetric display of electrostatically charged surfaces in the SHR-FF monomer. Most importantly, the asymmetry in the SHR-FF conformation at the monomer level was amplified in the higher-order packing and the fiber displayed a charged interface only in the quarter of the periphery along the long

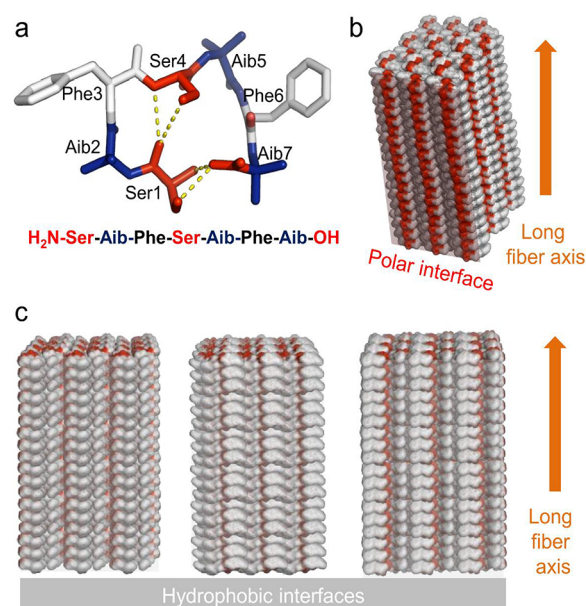


Figure 1. SHR-FF peptide assembly. (a) Sequence and crystal structure of SHR-FF. The polar segments are depicted in red, whereas the Aib residues are displayed as blue. (b) Higher order packing of SHR-FF reveals an asymmetric surface along the long axis of the fiber. Only one of the four interfaces along the long axis is polar in nature. (c) Three hydrophobic interfaces surround the periphery of the SHR-FF nanofibers.

axis due to Ser1 and the free terminals (Figure 1b). The rest of the surfaces displayed hydrophobic interfaces, as evident in Figure 1c. This analysis confirms that most of the fiber circumference is hydrophobic in nature with a small stretch of charged domain running along the fiber length. The extreme ends of the fibers also harbor polar surfaces owing to the presence of the Ser4 side chain and amide bonds (Figure S1).

Fabrication of Linear 1D Arrays Templated by Self-Assembled Peptide Fibers. The atomic-level understanding of the SHR-FF organization in the nanofibers inspired us to harness the asymmetry in surface charges to align nanoparticles through electrostatic interaction. We envisioned that the asymmetric nature of SHR-FF nanofibers has the potential to template the formation of single or few nanoparticle-wide 1D chains despite the fibers with diameters of more than 100 nm and afford a high persistence length nanoparticle array owing to its high crystallinity and rigidity. To test this hypothesis, a KAuCl₄ solution (5 mM) was added to the SHR-FF (5 mg mL⁻¹) nanofiber prepared in 100 mM HEPES buffer (pH 7.4) due to the later ability to reduce gold salt. As shown in Figure 2a, this method led to the in situ synthesis of AuNPs with varying sizes and diameters. Most importantly, as predicted, the AuNPs are aligned in linear chain-like arrangements and cover only a small fraction of fiber surface.

In addition, under the experimental conditions, the majority of synthesized AuNPs are attached to fibers confirming the strong interactions between them (Figure 2a, Figure S2). As mentioned before, the bottom-up fabrication of long, straight, and linear nanoparticle arrays are highly limited owing to the very low persistence length of the peptides or DNA templates. A simple visualization of Figure 2 and Figure S2 indicates that the straight chain-like arrangement of the plasmonic arrays has a high persistence length. To validate this, we analyzed the transmission electron microscope images of 100 nanofibers

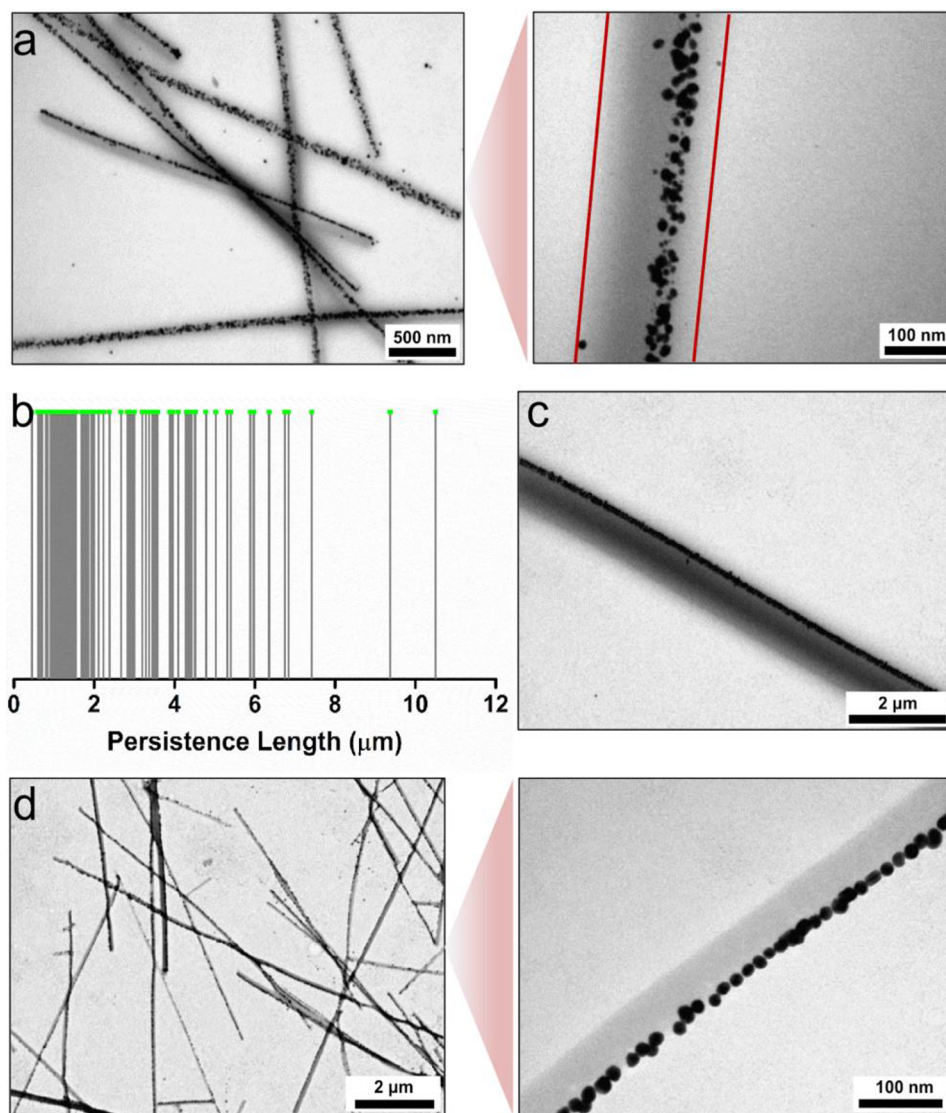


Figure 2. Linear 1D nanoparticle arrays with high persistence lengths. (a) In situ synthesis of AuNPs leads to the asymmetric linear 1D chain formation. The nanoparticles form a nearly continuous array and maintain excellent linearity. Zoomed in image of nanoparticles decorated fibril (right). (b) Distribution of persistence lengths of 1D nanoparticle arrays measured from TEM images by analyzing 100 AuNPs decorated nanofibers from three different experiments. (c) Decoration of preformed AuNPs (lipoic acid stabilized) in SHR-FF fiber template. (d) Decoration of preformed AuNPs (citrate stabilized) in SHR-FF fiber template. The representative zoomed image depicts the formation of a 1D chain with a single nanoparticle width.

decorated with AuNPs from three different experiments, and as shown in Figure 2b, the arrays indeed have the persistence lengths of several micrometers (average value is $2.7 \mu\text{m}$) and can extend to more than $10 \mu\text{m}$ (Figure 2b). This feature of SHR-FF fibers can be attributed to the crystalline nature of the assembly and the presence of the Aib residue which is known to introduce conformational rigidity into the peptide backbone. It is important to mention that the persistence lengths presented in Figure 2b are the minimal lengths, as the end of many fibers were not visible in the images and the actual average persistence length may have a higher value. To understand the nature of the interactions between the nanofibers and AuNPs, the ζ potential of the AuNPs in HEPES buffer was measured and it revealed -45 mV potential (Figure S3). This indicates a positive charge in the fibers, although the surface has negative (carboxy terminal), positive (amine terminal) and polar nonionized Ser1 side chains

(Figure 1a). The reduction of KAuCl_4 in the presence of nonassembled SHR-FF afforded AuNPs but without the higher order organization (Figure S4).

Although convenient, in situ synthesis of nanoparticles has a low versatility in terms of control over sizes, surface compositions, and functionalities. Thus, the asymmetric deposition of preformed nanoparticles with different functional groups will be preferable. To probe the versatile nature of SHR-FF template, we admixed commercially available citrate and lipoic acid stabilized AuNPs with diameters of 20 nm with SHR-FF fibers. In all samples, preferential asymmetric attachment of AuNPs was observed (Figure 2c,d and Figure S5), and the fibers as well as the metallic array maintained excellent linearity during the fabrication process. Noticeably, in addition to the multichain asymmetric assembly, a substantial population revealed the formation of linear and straight 1D chains with single nanoparticle width (Figure 2d). In a notable

study, Stupp and co-workers demonstrated that the supra-molecular assembly of asymmetric peptide amphiphiles leads to the formation of nanoribbons with asymmetric faces, as evidenced by the preferential but sparse attachment of AuNPs on only one face.⁴¹ In other studies, crystalline peptide and amino acid-based microstructures have been shown to possess facet-dependent asymmetric surfaces, amenable to asymmetric decoration of AuNPs as clusters.^{42,43} Evidently, the bottom-up formation of asymmetric self-assembled peptide nanostructures with the capability to template 1D chain-like organization of metal nanoparticles was not well explored. Most importantly, the presence of an asymmetric interface in the SHR-FF fiber allows the formation of a single or few nanoparticle-wide linear array with high persistence length even when the size of the AuNPs is only around 20 nm. We also measured the UV–vis spectra of 1D arrays prepared from preformed AuNPs to understand the nature of plasmonic coupling. The spectra revealed a high level of scattering from underlying peptide fibers, and this may have masked the signal arising from plasmonic arrays (Figure S6).

Insights about the Peptide Fiber and the Nanoparticle Interactions by All-atomistic MD Simulations.

To better understand the experimentally observed coupling of charged NPs with SHR-FF fibers, we studied the systems with all-atomistic MD simulations. Figure 3a shows a small, isolated crystallite formed by SHR-FF with an AuNP hovering above it in an aqueous solution. During the simulations, the neutral but highly polar 6912 peptides forming the crystal were partly stabilized from solvation by fixing the positions of heavy atoms. The AuNP (7 nm in diameter) coated with negatively charged citrate ligands (a surface density of 1.69 ligands/nm², AuNP net charge of $-780 e$) was placed above the crystallite. Sodium counterions (to balance the negative AuNP charge) and 0.1 M phosphate buffer at pH 7.4 were added to the aqueous solution. The dynamics of the negatively charged AuNP was largely driven by an electric field exerted by the non-centrosymmetric peptide crystal. The electric field is generated by electric dipole moments of peptides arranged in a parallel manner in the crystal, originating from the almost parallel orientations of the serine side groups in each monomer. Figure 3a,ii–iv reveals the electric field obtained for selected cross sections through the crystal by VMD. The potential at the top (bottom) left crystal corner has a highly positive (negative) value, thus attracting the negatively charged AuNP. In 5 ns simulations, the AuNP and the negative regions of the crystal became covered by adsorbed positive counterions. The partly screened electric field of the crystallite eventually attracted the AuNP toward one of its top corners with the most positive potential (indicated by the darkest shade of blue in Figure 3a,ii–iv), where the AuNP pivoted $\sim 7.4 \text{ \AA}$ above the surface (Figure 3a). Its average binding energy to the crystal normalized with respect to the number of peptides was -2.2 kcal/mol . When we placed the AuNP on the opposite side of the peptide crystal, there was a significant repulsion, where the AuNP diffused away from the peptide crystal (Figure S7). The attraction of the charged AuNP and the peptide crystal is merely the interaction of a monopole to a dipole, in which the monopole is attracted to the end of the dipole with opposite charge. These results support the experimental observations, showing that the AuNPs coalesce along the crystal edges and only a fraction of the SHR-FF fibril surface is amenable to charge complementary interactions.

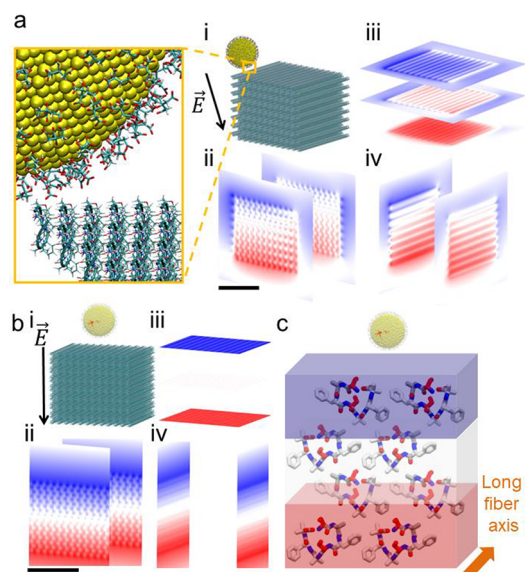


Figure 3. AuNP positions with respect to SHR-FF crystal and volumetric slices of electric field exerted by the SHR-FF crystal. Dark blue values represent regions with a strongly positive electric field, and dark red regions represent regions with a strongly negative electric field. (a) (i) SHR-FF crystal with a citrate ligands-covered AuNP stabilized above it after 26 ns (insight image shows details of peptide crystal and AuNP); approximate direction of electric field exerted by the crystal; (ii) electric field slices along the *a* axis; (iii) electric field slices along the *b* axis; and (iv) electric field slices along the *c* axis. Scale bar in (a) represents 10 nm for (i–iv). (b) (i) 41 ns trajectory of center of mass of AuNPs along crystals extended by PBC and electric field exerted by crystals; (ii) electric field slices along the *a* axis; (iii) electric field slices along the *b* axis; and (iv) electric field slices along the *c* axis. Scale bar represents 10 nm (for i–iv). (c) Schematic diagram showing the organization of SHR-FF with respect to the charge distribution in the nanofibers. Only one layer of SHR-FF molecules is displayed for clarity.

Next, we simulated the same crystal with periodic boundary conditions applied to model an infinite crystal surface. Since the electric field above the surface became uniform (Figures 3b), the interaction energy between the AuNP and the crystal only depends on their mutual separation. Therefore, once the AuNP got close to the crystal surface, it randomly hovered within 4–17 Å above it (Figure 3b,i). Its average binding energy to the crystal normalized with respect to the number of peptides was -5.9 kcal/mol . As shown in Figure 3b,i, AuNP was attracted only to one side of the infinite crystal. As evident from the simulations, the dipole in the peptide crystal originates from the overall organization of SHR-FF molecules. All the residues including serine and amide backbones contribute to different extents to generate the observed dipole (Figure 3c).

Versatility of Peptide Fibrils to Template 1D Array of Diverse Types of Nanoparticles. The extensive MD simulations confirm that nanoparticles can only access a narrow zone of the SHR-FF fibril surface through charge complementary interaction. As this process is nonspecific in nature, it can be inferred that SHR-FF asymmetric template can be employed beyond AuNPs. To explore this, we selected super paramagnetic nanoparticles (SNPs) owing to their multifaceted applications.^{7,44} Following a similar protocol, bare preformed SNPs with negative surface charge were mixed

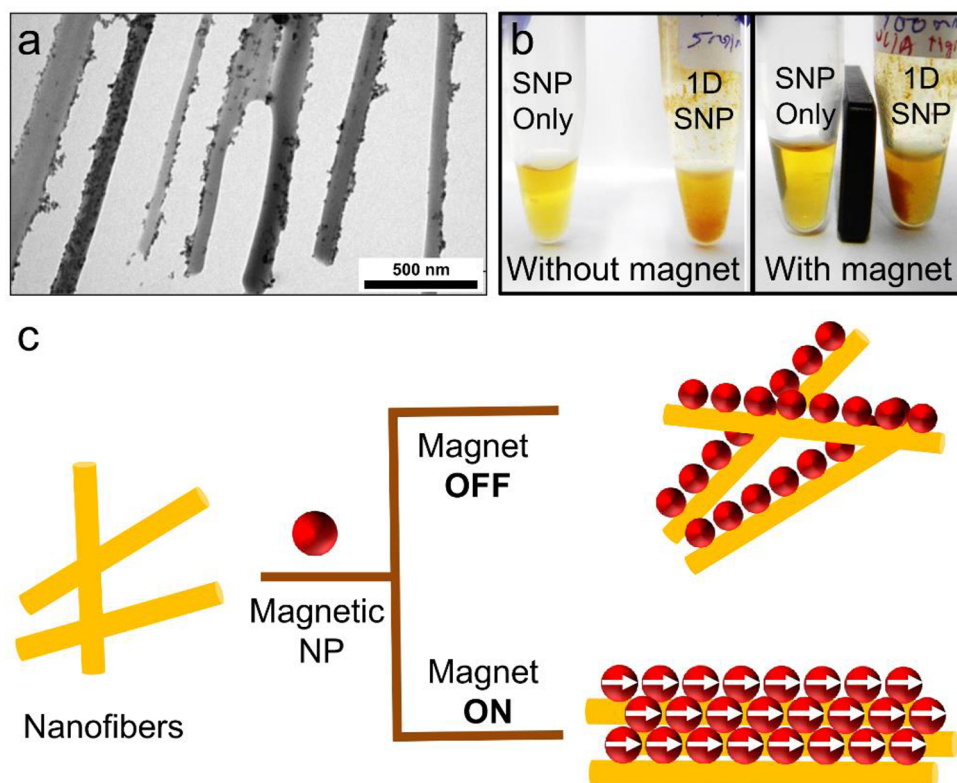


Figure 4. Versatility of SHR-FF fibrillar template. (a) 1D chain-like assembly of SNPs. (b) Comparison of cumulative magnetic properties of 1D chains and dispersed nanoparticles in the absence or presence of magnetic field, respectively. (c) Schematic illustration of mechanism of magnetic effect in the presence and absence of an external magnet.

with SHR-FF nanofibers. The TEM images revealed the formation of a 1D nanochain reminiscent of AuNP chains, validating the template's versatility (Figure 4a). It is known that in the presence of an external magnetic field, a temporary magnetic moment is generated in SNPs, and when arranged in 1D architecture, such a magnetic moment is aligned in the direction of the long axis of the fibers, thus affording a very high net magnetic moment.⁴⁵ To demonstrate this effect, we placed the 1D SNPs in a static magnetic field. As expected, the SNPs array underwent further assembly and pulled toward the external magnet, whereas in the absence of an external field, they remain well dispersed in the solution (Figure 4b). It can be surmised that the net high magnetic moment of the individual 1D SNPs arrays favored the lateral association of fibers in which the individual magnetic nanoparticle aligned in offset geometry (Figure 4c), whereas in the absence of an external magnet, the individual SNPs magnetic moments as well as the 1D array have random orientation and do not reveal any higher order aggregation (Figure 4c). We have also placed the isolated SNPs under the same static magnetic field, and as shown in Figure 4b, the SNPs remained completely dispersed, further confirming the very high net magnetic moments of the 1D SNPs arrays. Literature reports suggest that the net magnetic moments and the persistence length of the 1D array are correlated.⁴⁵ Accordingly, excellent aggregation propensity of the 1D SNPs under weak magnetic field can be attributed to the high persistence length of the SHR-FF fiber templated 1D SNPs. This study indicates that the SHR-FF templated magnetic chain can be advantageous for magnetic separation in low magnetic fields.

CONCLUSION

In conclusion, we have developed a self-assembling peptide template that allows the formation of linear 1D nanoparticle chains with high persistence length. The linearity of the 1D chains was attributed to the crystallinity of the nanofibers and asymmetric display of the polar surface along the long axis of fibers. This asymmetric nature further facilitated the assembly of single nanoparticle-wide 1D chains in which the fibrillar template has a much larger total surface area than the nanoparticle sizes. The rigid linear chain-like organization of nanoparticles demonstrated in this study will be highly beneficial for the construction of ordered 2D arrays.^{8,46} Moreover, detailed MD simulations confirm the role of the nonspecific electrostatic nature of interactions which allows 1D chain-like assembly of nanostructures with diverse features such as magnetic and gold nanoparticles. It can be envisioned that the control over the diameter and length of the SHR-FF fiber can be harnessed to afford highly homogeneous single nanoparticle-wide 1D chains with high persistence lengths comparable to lithography and DNA nanotechnology-based approaches but with tremendous cost-effectiveness. Finally, the incorporation of Aib in β -sheet-based peptide design has the potential to afford fibrillar assembly with an asymmetric surface.

METHODS

Self-Assembly of SHR-FF. SHR-FF was purchased from Pepton, Inc. (South Korea). The lyophilized peptide powder was dissolved in 100 mM HEPES buffer at pH 7.4 at a concentration of 5 mg mL⁻¹ and stored in a sealed plastic vial. The sample was incubated at room temperature for a duration of 5–7 days to allow the formation of

fibrils. The resulting fibrils have been used to study the interaction with metal nanoparticles.

Interactions of SHR-FF Fibril Templates with AuNPs. KAuCl_4 was dissolved in an ultrapure solution in the appropriate concentration. The KAuCl_4 solution was then added to the preformed SHR-FF fibril (5 mg mL^{-1}) prepared in 100 mM HEPES buffer at pH 7.4 as discussed above. The volume of the added KAuCl_4 solution was maintained at 3% with respect to the initial volume of the original SHR-FF solution. The solution was agitated at 200 rpm for 2 h followed by 400 rpm for 2 h in an orbital shaker. The completion of the process was indicated by a change in solution color from golden yellow to purple. The AuNP decorated SHR-FF was stored at 4°C for further analysis. The ζ potential measurement was performed by preparing the AuNPs in 100 mM HEPES buffer (pH = 7.4) in the absence of SHR-FF fibers (Zetasizer Nano ZS, Malvern Instruments).

To study the interactions of SHR-FF fibers with preformed AuNPs, the preformed SHR-FF fibril solution was centrifuged at 2000 rpm for 10 min. The supernatant was removed. The pellet containing SHR-FF fibril was resuspended in the appropriate volume of preformed AuNPs (Au concentration 1 mg mL^{-1}) in water to reach a final concentration of $\sim 5 \text{ mg mL}^{-1}$ of SHR-FF. Preformed AuNPs with a diameter of 20 nm were purchased from nanoComposix, USA. The commercially procured preformed AuNPs contain citrate and lipoic acid as stabilizing agents.

UV-vis spectra of only preformed AuNPs (Au concentration 1 mg mL^{-1}) and solution containing the 1D arrays as prepared above were measured in a 96-well plate containing $200 \mu\text{L}$ of respective solutions. The spectra were collected in a BMG Labtech microplate reader.

Interactions of SHR-FF Fibril Templates with Magnetic Nanoparticles. SHR-FF was prepared in a buffer solution as described above. The sample was centrifuged at 2000 rpm for 10 min. The supernatant was removed, and the pellet containing SHR-FF fibril was resuspended in ultrapure water. To this, $20 \mu\text{L}$ (buffer:magnetic nanoparticle solution = 5:1 (v/v)) of magnetic nanoparticle solution (25 mg mL^{-1} , diphosphate functionalized, Chemicell GmbH, Germany) was added. The sample was agitated in an orbital shaker at 200 rpm for 4 h. The deposited nanoparticle arrays were washed twice with ultrapure water following the above centrifugation protocol to remove the secondary aggregates of the nanoparticles from 1D array. The final solution was stored at 4°C for further analysis.

Transmission Electron Microscopy. The SHR-FF fibers with or without the nanoparticles were analyzed by transmission electron microscopy. Before sample preparation, SHR-FF fibers decorated with magnetic nanoparticles were washed twice with ultrapure water following the centrifuge method discussed above, whereas AuNPs containing samples were imaged without any postprocessing. Seven μL of the solution was placed on a 400 mesh copper grids. After 1 min, excess fluids were blotted. Samples were viewed using a JEOL 1200EX electron microscope operating at 80 kV.

Molecular Dynamics Simulations. MD simulations were performed with NAMD2.12 software. The natural amino acids of the peptide and the solvent were described with the CHARMM36 protein force field.^{47–49} The Aib amino acid was described with the generalized CHARMM force field,^{49,50} and the parameters were determined via the CGenFF ParamChem web interface.^{51,52} In all the simulations, the particle-mesh Ewald method^{53,54} was used for evaluation of long-range Coulomb interactions. The time step was set to 1.0 fs, and long-range interactions were evaluated every 1 (van der Waals) and 2 (Coulombic) time steps. The simulations for completely solvated crystals were performed in the NPT ensemble, and the broad crystal was performed at NAPT ensemble. The area for the NAPT ensemble was taken from unit cell parameters of the crystal. The simulations had temperature $T = 310 \text{ K}$, constant pressure of $p = 1 \text{ atm}$, and a Langevin constant of $\gamma_{\text{Lang}} = 1.00 \text{ ps}^{-1}$. All simulations were performed with a 7 nm AuNP particle and had citrate ligands randomly distributed with surface density $1.69 \text{ ligands/nm}^2$. Systems were simulated in 0.1 M phosphate buffer solution of pH 7.4 determined by the ratio of H_2PO_4^- and HPO_4^{2-} ions to screen image peptide crystals.

The systems were first minimized for 5000 steps. Then, they were heated to the desired temperature, at 5 steps/K for 2000 steps, where they were equilibrated. In the first simulation, production runs were taken even when the AuNP was attracted to the free counterions in the solution more strongly than the crystal. In all other simulations, we waited for enough for counterions to be attracted to the AuNP and then forced the AuNP to the crystal surface before taking the production runs.

ASSOCIATED CONTENT

Supporting Information

The Supporting Information is available free of charge at <https://pubs.acs.org/doi/10.1021/acsnano.2c06082>.

Crystal structure showing the extreme end of fiber. The ζ potential graph, TEM images in low and high magnification, UV-vis spectra of AuNPs under different conditions. MD simulations images (PDF)

AUTHOR INFORMATION

Corresponding Authors

Sudipta Mondal – Department of Biotechnology, National Institute of Technology Durgapur, Durgapur 713209, India;

orcid.org/0000-0002-1146-8659;

Email: sudipta.mondal@bt.nitdgp.ac.in

Ehud Gazit – Shmunis School of Biomedicine and Cancer Research, Dr. George S. Wise Faculty of Life Sciences, Tel Aviv University, Tel Aviv–Yafo 69978, Israel;

Email: ehudg@post.tau.ac.il

Authors

Pavel Rehak – Chemistry, Physics, Pharmaceutical Sciences, Chemical Engineering, University of Illinois at Chicago, Chicago, Illinois 60607, United States

Nandita Ghosh – Department of Biotechnology, National Institute of Technology Durgapur, Durgapur 713209, India

Petr Král – Chemistry, Physics, Pharmaceutical Sciences, Chemical Engineering, University of Illinois at Chicago, Chicago, Illinois 60607, United States; orcid.org/0000-0003-2992-9027

Complete contact information is available at:

<https://pubs.acs.org/doi/10.1021/acsnano.2c06082>

Author Contributions

S.M. and E.G. conceived and designed the experiments. S.M. and N.G. performed the experiments. P.K. and P.R. performed the simulation experiments. All authors contributed to the writing and proofreading of the manuscript.

Notes

The authors declare no competing financial interest.

ACKNOWLEDGMENTS

This work was supported by DST-SERB research grant (SRG/2019/001058) to S.M. and the European Research Council under the European Union Horizon 2020 research and innovation program (no. 694426) to E.G. N.G. thanks DST-SERB research grant (SRG/2019/001058) for the fellowship. The authors thank the members of the Gazit laboratory for helpful discussions.

REFERENCES

- (1) Wang, W.; Ramezani, M.; Väkeväinen, A. I.; Törmä, P.; Rivas, J. G.; Odom, T. W. The rich photonic world of plasmonic nanoparticle arrays. *Mater. Today* **2018**, *21*, 303–314.

- (2) Nie, Z.; Petukhova, A.; Kumacheva, E. Properties and emerging applications of self-assembled structures made from inorganic nanoparticles. *Nat. Nanotechnol.* **2010**, *5*, 15–25.
- (3) Kitching, H.; Shiers, M. J.; Kenyon, A. J.; Parkin, I. P. Self-assembly of metallic nanoparticles into one dimensional arrays. *J. Mater. Chem. A* **2013**, *1*, 6985–6999.
- (4) Halas, N. J.; Lal, S.; Chang, W.-S.; Link, S.; Nordlander, P. Plasmons in Strongly Coupled Metallic Nanostructures. *Chem. Rev.* **2011**, *111*, 3913–3961.
- (5) Février, M.; Gogol, P.; Aassime, A.; Mégy, R.; Delacour, C.; Chelnokov, A.; Apuzzo, A.; Blaize, S.; Lourtioz, J.-M.; Dagens, B. Giant Coupling Effect between Metal Nanoparticle Chain and Optical Waveguide. *Nano Lett.* **2012**, *12*, 1032–1037.
- (6) Kravets, V. V.; Ocola, L. E.; Khalavka, Y.; Pinchuk, A. O. Polarization and distance dependent coupling in linear chains of gold nanoparticles. *Appl. Phys. Lett.* **2015**, *106*, 053104.
- (7) Kim, J.; Chung, S. E.; Choi, S.-E.; Lee, H.; Kim, J.; Kwon, S. Programming magnetic anisotropy in polymeric microactuators. *Nat. Mater.* **2011**, *10*, 747–752.
- (8) Maier, S. A.; Kik, P. G.; Atwater, H. A.; Meltzer, S.; Harel, E.; Koel, B. E.; Requicha, A. A. G. Local detection of electromagnetic energy transport below the diffraction limit in metal nanoparticle plasmon waveguides. *Nat. Mater.* **2003**, *2*, 229–232.
- (9) Catherall, T.; Huskisson, D.; McAdams, S.; Vijayaraghavan, A. Self-assembly of one dimensional DNA-templated structures. *J. Mater. Chem. C* **2014**, *2*, 6895–6920.
- (10) Jiang, L.; Wang, W.; Fuchs, H.; Chi, L. One-Dimensional Arrangement of Gold Nanoparticles with Tunable Interparticle Distance. *Small* **2009**, *5*, 2819–2822.
- (11) Miele, E.; Raj, S.; Baraissov, Z.; Král, P.; Mírsaidov, U. Dynamics of Templated Assembly of Nanoparticle Filaments within Nanochannels. *Adv. Mater.* **2017**, *29*, 1702682.
- (12) Xia, D.; Ku, Z.; Lee, S. C.; Brueck, S. R. J. Nanostructures and Functional Materials Fabricated by Interferometric Lithography. *Adv. Mater.* **2011**, *23*, 147–179.
- (13) Dahlhaus, D.; Franzka, S.; Hasselbrink, E.; Hartmann, N. 1D Nanofabrication with a Micrometer-Sized Laser Spot. *J. Mater. Chem. B* **2006**, *6*, 2358–2361.
- (14) Warner, M. G.; Hutchison, J. E. Linear assemblies of nanoparticles electrostatically organized on DNA scaffolds. *Nat. Mater.* **2003**, *2*, 272–277.
- (15) Yang, Z.; Liu, H.; Liu, D. Spatial regulation of synthetic and biological nanoparticles by DNA nanotechnology. *NPG Asia Mater.* **2015**, *7*, e161.
- (16) Vogele, K.; List, J.; Pardatscher, G.; Holland, N. B.; Simmel, F. C.; Pirzer, T. Self-Assembled Active Plasmonic Waveguide with a Peptide-Based Thermomechanical Switch. *ACS Nano* **2016**, *10*, 11377–11384.
- (17) Wang, P.; Huh, J. H.; Park, H.; Yang, D.; Zhang, Y.; Zhang, Y.; Lee, J.; Lee, S.; Ke, Y. DNA Origami Guided Self-Assembly of Plasmonic Polymers with Robust Long-Range Plasmonic Resonance. *Nano Lett.* **2020**, *20*, 8926–8932.
- (18) Kuzyk, A.; Schreiber, R.; Fan, Z.; Pardatscher, G.; Roller, E. M.; Högele, A.; Simmel, F. C.; Gorovov, A. O.; Liedl, T. DNA-based self-assembly of chiral plasmonic nanostructures with tailored optical response. *Nature* **2012**, *483*, 311–314.
- (19) Lampel, A.; McPhee, S. A.; Park, H. A.; Scott, G. G.; Humagain, S.; Hekstra, D. R.; Yoo, B.; Frederix, P. W. J. M.; Li, T. D.; Abzalimov, R. R.; Greenbaum, S. G.; Tuttle, T.; Hu, C.; Bettinger, C. J.; Ulijn, R. V. Polymeric peptide pigments with sequence-encoded properties. *Science* **2017**, *356*, 1064–1068.
- (20) Huang, R. H.; Nayeem, N.; He, Y.; Morales, J.; Graham, D.; Klajn, R.; Contel, M.; O'Brien, S.; Ulijn, R. V. Self-Complementary Zwitterionic Peptides Direct Nanoparticle Assembly and Enable Enzymatic Selection of Endocytic Pathways. *Adv. Mater.* **2022**, *34*, 2104962.
- (21) Pappas, C. G.; Shafi, R.; Sasselli, I. R.; Siccardi, H.; Wang, T.; Narang, V.; Abzalimov, R.; Wijerathne, N.; Ulijn, R. V. Dynamic peptide libraries for the discovery of supramolecular nanomaterials. *Nat. Nanotechnol.* **2016**, *11*, 960–967.
- (22) Bera, S.; Mondal, S.; Xue, B.; Shimon, L. J. W.; Cao, Y.; Gazit, E. Rigid helical-like assemblies from a self-aggregating tripeptide. *Nat. Mater.* **2019**, *18*, 503–509.
- (23) Mondal, S.; Gazit, E. The Self-Assembly of Helical Peptide Building Blocks. *ChemNanoMat* **2016**, *2*, 323–332.
- (24) Vila-Liarte, D.; Kotov, N. A.; Liz-Marzán, L. M. Template-assisted self-assembly of achiral plasmonic nanoparticles into chiral structures. *Chem. Sci.* **2022**, *13*, 595–610.
- (25) Teng, J.; Peydayesh, M.; Lu, J.; Zhou, J.; Benedek, P.; Schäublin, R. E.; You, S.; Mezzenga, R. Amyloid-Templated Palladium Nanoparticles for Water Purification by Electroreduction. *Angew. Chem., Int. Ed.* **2022**, *61*, 202116634.
- (26) Burkett, S. L.; Mann, S. Spatial organization and patterning of gold nanoparticles on self-assembled biolipid tubular templates. *Chem. Commun.* **1996**, 321–322.
- (27) Guterman, T.; Ing, N. L.; Fleischer, S.; Rehak, P.; Basavalingappa, V.; Hunashal, Y.; Dongre, R.; Raghobama, S.; Král, P.; Dvir, T.; Hochbaum, A. I.; Gazit, E. Electrical Conductivity, Selective Adhesion, and Biocompatibility in Bacteria-Inspired Peptide-Metal Self-Supporting Nanocomposites. *Adv. Mater.* **2019**, *31*, 1807285.
- (28) Tian, Y.; Zhang, H. V.; Kiick, K. L.; Saven, J. G.; Pochan, D. J. Fabrication of One- and Two-Dimensional Gold Nanoparticle Arrays on Computationally Designed Self-Assembled Peptide Templates. *Chem. Mater.* **2018**, *30*, 8510–8520.
- (29) Fu, X.; Wang, Y.; Huang, L.; Sha, Y.; Gui, L.; Lai, L.; Tang, Y. Assemblies of Metal Nanoparticles and Self-Assembled Peptide Fibrils—Formation of Double Helical and Single-Chain Arrays of Metal Nanoparticles. *Adv. Mater.* **2003**, *15*, 902–906.
- (30) Sharma, N.; Top, A.; Kiick, K. L.; Pochan, D. J. One-dimensional gold nanoparticle arrays by electrostatically directed organization using polypeptide self-assembly. *Angew. Chem., Int. Ed.* **2009**, *48*, 7078–7082.
- (31) Deschaume, O.; De Roo, B.; Van Bael, M. J.; Locquet, J.-P.; Van Haesendonck, C.; Bartic, C. Synthesis and Properties of Gold Nanoparticle Arrays Self-Organized on Surface-Deposited Lysozyme Amyloid Scaffolds. *Chem. Mater.* **2014**, *26*, 5383–5393.
- (32) Bae, A.-H.; Numata, M.; Hasegawa, T.; Li, C.; Kaneko, K.; Sakurai, K.; Shinkai, S. 1D Arrangement of Au Nanoparticles by the Helical Structure of Schizophyllan: A Unique Encounter of a Natural Product with Inorganic Compounds. *Angew. Chem., Int. Ed.* **2005**, *44*, 2030–2033.
- (33) Kang, E. S.; Kim, Y.-T.; Ko, Y.-S.; Kim, N. H.; Cho, G.; Huh, Y. H.; Kim, J.-H.; Nam, J.; Thach, T. T.; Youn, D.; Kim, Y. D.; Yun, W. S.; DeGrado, W. F.; Kim, S. Y.; Hammond, P. T.; Lee, J.; Kwon, Y.-U.; Ha, D.-H.; Kim, Y. H. Peptide-Programmable nanoparticle superstructures with tailored electrocatalytic activity. *ACS Nano* **2018**, *12*, 6554–6562.
- (34) Pazos, E.; Sleep, E.; Rubert Pérez, C. M.; Lee, S. S.; Tantakitti, F.; Stupp, S. I. Nucleation and Growth of Ordered Arrays of Silver Nanoparticles on Peptide Nanofibers: Hybrid Nanostructures with Antimicrobial Properties. *J. Am. Chem. Soc.* **2016**, *138*, 5507–5510.
- (35) Song, C.; Wang, Y.; Rosi, N. L. Peptide-Directed Synthesis and Assembly of Hollow Spherical CoPt Nanoparticle Superstructures. *Angew. Chem., Int. Ed.* **2013**, *52*, 3993–3995.
- (36) Merg, A. D.; Slocik, J.; Blaber, M. G.; Schatz, G. C.; Naik, R.; Rosi, N. L. Adjusting the metrics of 1-D helical gold nanoparticle superstructures using multivalent peptide conjugates. *Langmuir* **2015**, *31*, 9492–9501.
- (37) Shen, Y.; Posavec, L.; Bolisetty, S.; Hilty, F. M.; Nyström, G.; Kohlbrecher, J.; Hilbe, M.; Rossi, A.; Baumgartner, J.; Zimmermann, M. B.; Mezzenga, R. Amyloid fibril systems reduce, stabilize and deliver bioavailable nanosized iron. *Nat. Nanotechnol.* **2017**, *12*, 642–647.
- (38) Fakhri, N.; Tsyboulski, D. A.; Cognet, L.; Weisman, R. B.; Pasquali, M. Diameter-dependent bending dynamics of single-walled

carbon nanotubes in liquids. *Proc. Natl. Acad. Sci. U.S.A.* **2009**, *106*, 14219–14223.

(39) Mondal, S.; Jacoby, G.; Sawaya, M. R.; Arnon, Z. A.; Adler-Abramovich, L.; Rehak, P.; Vuković, L.; Shimon, L. J. W.; Král, P.; Beck, R.; Gazit, E. Transition of metastable cross- α crystals into cross- β fibrils by β -turn flipping. *J. Am. Chem. Soc.* **2019**, *141*, 363–369.

(40) Mondal, S.; Adler-Abramovich, L.; Lampel, A.; Bram, Y.; Lipstman, S.; Gazit, E. Formation of functional super-helical assemblies by constrained single heptad repeat. *Nat. Commun.* **2015**, *6*, 8615–8624.

(41) Yu, Z.; Tantakitti, F.; Palmer, L. C.; Stupp, S. I. Asymmetric Peptide Nanoribbons. *Nano Lett.* **2016**, *16*, 6967–6974.

(42) Yoo, S. H.; Eom, T.; Kwon, S.; Gong, J.; Kim, J.; Cho, S. J.; Driver, R. W.; Lee, Y.; Kim, H.; Lee, H.-S. Foldection as a core material with anisotropic surface characteristics. *J. Am. Chem. Soc.* **2015**, *137*, 2159–2162.

(43) Fujiki, Y.; Tokunaga, N.; Shinkai, S.; Sada, K. Anisotropic decoration of gold nanoparticles onto specific crystal faces of organic single crystals. *Angew. Chem., Int. Ed.* **2006**, *45*, 4764–4767.

(44) Mehdizadeh Taheri, S.; Michaelis, M.; Friedrich, T.; Förster, B.; Drechsler, M.; Römer, F. M.; Bösecke, P.; Narayanan, T.; Weber, B.; Rehberg, I.; Rosenfeldt, S.; Förster, S. Self-assembly of smallest magnetic particles. *Proc. Natl. Acad. Sci. U.S.A.* **2015**, *112*, 14484–14489.

(45) Sim, S.; Miyajima, D.; Niwa, T.; Taguchi, H.; Aida, T. Tailoring Micrometer-Long High-Integrity 1D Array of Superparamagnetic Nanoparticles in a Nanotubular Protein Jacket and Its Lateral Magnetic Assembling Behavior. *J. Am. Chem. Soc.* **2015**, *137*, 4658–4661.

(46) Lee, S.-W.; Mao, C.; Flynn, C. E.; Belcher, A. M. Ordering of quantum dots using genetically engineered viruses. *Science* **2002**, *296*, 892–895.

(47) MacKerell Jr, A. D.; Bashford, D.; Bellott, M.; Dunbrack Jr, R. L.; Evanseck, J. D.; Field, M. J.; Fischer, S.; Gao, J.; Guo, H.; Ha, S.; Joseph-McCarthy, D.; Kuchnir, L.; Kuczera, K.; Lau, F. T. K.; Mattos, C.; Michnick, S.; Ngo, T.; Nguyen, D. T.; Prodhom, B.; Reiher, W. E.; Roux, B.; Schlenkrich, M.; Smith, J. C.; Stote, R.; Straub, J.; Watanabe, M.; Wiórkiewicz-Kuczera, J.; Yin, D.; Karplus, M. All-atom empirical potential for molecular modeling and dynamics studies of proteins. *J. Phys. Chem. B* **1998**, *102*, 3586–3616.

(48) MacKerell, A. D., Jr; Feig, M.; Brooks, C. L. Improved treatment of the protein backbone in empirical force fields. *J. Am. Chem. Soc.* **2004**, *126*, 698–699.

(49) Best, R. B.; Zhu, X.; Shim, J.; Lopes, P. E. M.; Mittal, J.; Feig, M.; MacKerell, A. D., Jr Optimization of the additive CHARMM all-atom protein force field targeting improved sampling of the backbone ϕ , ψ and side-chain χ_1 and χ_2 dihedral angles. *J. Chem. Theory Comput.* **2012**, *8*, 3257–3273.

(50) Vanommeslaeghe, K.; Hatcher, E.; Acharya, C.; Kundu, S.; Zhong, S.; Shim, J.; Darian, E.; Guvench, O.; Lopes, P.; Vorobyov, I.; Mackerell, A. D. CHARMM general force field: A force field for drug-like molecules compatible with the CHARMM all-atom additive biological force fields. *J. Comput. Chem.* **2009**, *31*, 671–690.

(51) Vanommeslaeghe, K.; MacKerell, A. D., Jr Automation of the CHARMM General Force Field (CGenFF) I: bond perception and atom typing. *J. Chem. Inf. Model.* **2012**, *52*, 3144–3154.

(52) Vanommeslaeghe, K.; Raman, E. P.; MacKerell, A. D. Automation of the CHARMM General Force Field (CGenFF) II: assignment of bonded parameters and partial atomic charges. *J. Chem. Inf. Model.* **2012**, *52*, 3155–3168.

(53) Darden, T.; York, D.; Pedersen, L. Particle mesh Ewald: An $N \log(N)$ method for Ewald sums in large systems. *J. Chem. Phys.* **1993**, *98*, 10089–10092.

(54) Humphrey, W.; Dalke, A.; Schulten, K. VMD: visual molecular dynamics. *J. Mol. Graph.* **1996**, *14*, 33–38.

Recommended by ACS

Three-Dimensional Printing of Dipeptides with Spatioselective Programming of Crystallinity for Multilevel Anticounterfeiting

Jihyuk Yang, Ji Tae Kim, *et al.*

SEPTEMBER 29, 2022

NANO LETTERS

READ 

Polyethyleneimine-Enabled Tunable Electrostatic Nanoparticle Assemblies on Ultrathin Protein Nanofibers for Plasmonics-Based Solar Energy Harvesting

Lin Wang, Chuanbin Mao, *et al.*

DECEMBER 29, 2021

ACS APPLIED NANO MATERIALS

READ 

Connected Peptide Modules Enable Controlled Co-Existence of Self-Assembled Fibers Inside Liquid Condensates

Ankit Jain, Rein V. Ulijn, *et al.*

AUGUST 10, 2022

JOURNAL OF THE AMERICAN CHEMICAL SOCIETY

READ 

Kinetic and Thermodynamic Driving Factors in the Assembly of Phenylalanine-Based Modules

Dor Zaguri, Ehud Gazit, *et al.*

OCTOBER 25, 2021

ACS NANO

READ 

Get More Suggestions >